

Estimation of the amount of retained austenite in austempered ductile irons using neural networks

M.A. Yescas^a, H.K.D.H. Bhadeshia^{a,*}, D.J. MacKay^b

^a *Department of Materials Science and Metallurgy, University of Cambridge, Pembroke Street, Cambridge CB2 3QZ, UK*

^b *Cavendish Laboratory, University of Cambridge, Madingley Road, Cambridge CB3 0HE, UK*

Received 21 August 2000; received in revised form 9 November 2000

Abstract

Many of the properties of austempered ductile iron depend on the austenite which is retained following the bainite reaction. A neural network model within a Bayesian framework has been created using published data to model the retained austenite content. The model allows the quantity of retained austenite to be estimated as a function of the chemical composition and heat treatment parameters. The computer programs associated with the work have been made freely available (<http://www.msm.cam.ac.uk/map/mapmain.html>) © 2001 Elsevier Science B.V. All rights reserved.

Keywords: Retained austenite; Austempered; Bainite; Ductile iron; Neural networks

1. Introduction

Austempered ductile iron (ADI) has a microstructure containing spheroidal graphite embedded in a matrix which is in general a mixture of bainitic ferrite, austenite and some martensite [1–3]. The bainitic ferrite is generated by the isothermal transformation of austenite in the bainite transformation temperature range; this heat treatment is known as austempering.

The large concentration of silicon typically present in graphitic cast irons has a key role in the development of the microstructure of austempered irons. The silicon hinders the precipitation of carbides during the bainite transformation [4,5]. The austempering time must ensure that the formation of bainitic ferrite adequately enriches the residual austenite with carbon, allowing much of it to be retained to room temperature. Unfortunately, prolonged austempering causes the decomposition of the residual austenite into a mixture of carbides and ferrite [6]. This is detrimental to the mechanical properties.

The austempering process is therefore conventionally defined in two stages [7]. The end of the first stage corresponds to the maximisation of the fraction of bainitic ferrite and the enrichment of the austenite, the second with the onset of carbide precipitation. The time interval between these two stages is the heat treatment window (Fig. 1). The effect of austempering can be optimised within the confines of this window: too short an austempering time leads to an inadequate enrichment of the austenite and hence a lower retained austenite content. Austempering beyond the commencement of stage II causes carbide precipitation and once again, a reduction in the retained austenite content. The extent of the heat treatment window is reduced by the presence of inevitable solidification-induced chemical segregation, since the transformations occur at different times in different regions of the sample. It thus becomes difficult, if not impossible, to define an ideal austempering time for the whole of the cast iron component.

The problem of designing these cast irons clearly involves many variables and considerable complexity. The purpose of the work presented here was to develop a quantitative model which makes possible the estimation of retained austenite content as a function of all these variables, using a neural network technique within a Bayesian framework [8].

* Corresponding author. Tel.: +44-1223-334301; fax: +44-1223-334567.

E-mail address: hkdb@cus.cam.ac.uk (H.K.D.H. Bhadeshia).

2. The technique

A neural network is a general method of regression analysis in which a flexible non-linear function is fitted to experimental data, the details of which have been reviewed extensively [8–10]. It is nevertheless worth emphasising some of the features of the particular method used here, which is due to MacKay [11,12]. The method, in addition to providing an indication of the perceived level of noise in the output, gives error bars representing the uncertainty in the fitting parameters. The method recognises that there are many functions which can be fitted or extrapolated into uncertain regions of the input space, without excessively compromising the fit in adjacent regions which are rich in accurate data. Instead of calculating a unique set of weights, a probability distribution of sets of weights is used to define the fitting uncertainty. The error bars therefore become large when data are sparse or locally noisy.

The Bayesian framework for neural networks has a further advantage. The significance of the input variables is automatically quantified [11,12]. Consequently

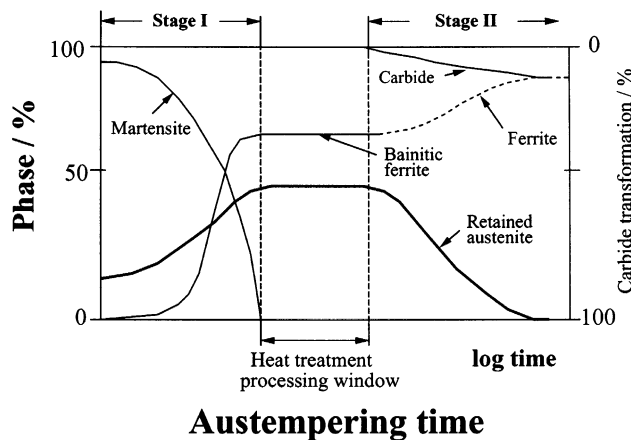


Fig. 1. Schematic representation of the development of microstructure during austempering, together with an illustration of the 'processing window'. Martensite is present only when the sample is cooled to room temperature before the austempering has been completed.

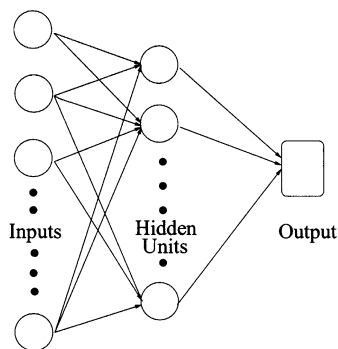


Fig. 2. The structure of the network.

the significance, perceived by the model of each input variable can be compared against metallurgical experience.

The general form of the model is as follows, with y representing the output variable and x_j the set of inputs.

$$y = \sum_i w_{ij}^{(2)} h_i + \theta^{(2)}, \text{ where } h_i = \tan h \left(\sum_j w_{ij}^{(1)} x_j + \theta_i^{(1)} \right). \quad (1)$$

The subscript i represents the hidden units (Fig. 2), the θ terms are biases and the weights. Thus, the statement of Eq. (1) together with the weights and coefficients defines the function giving the output as a function of the inputs.

A potential difficulty with the use of powerful regression methods is the possibility of overfitting data. To avoid this, the experimental data can be divided into two sets, a training data set and a test data set. The model is produced using only the training data. The test data are then used to check that the model behaves itself when presented with previously unseen data. The training process involves a search for the optimum non-linear relationship between the input and the output data and is computer intensive. Once the network is trained, estimation of the outputs for any given set of inputs is very fast.

3. The variables

The analysis is based on published data and is therefore limited to quantities that are readily measured and frequently reported. For example, in order to predict the quantity of retained austenite it would be ideal to include the fraction of bainite as an input, but this is rarely measured in practice. Therefore, a pragmatic set of variables must be chosen which implicitly contain all the information needed to estimate the amount of retained austenite.

The set of inputs (Table 1) therefore included the detailed chemical composition in wt.%, the austenitisation temperature in °C and time in min (T_γ and t_γ , respectively), and the austempering temperature and time (T_A and t_A , respectively). This is almost all that is necessary to define the retained austenite volume fraction ($V_{r\gamma}$). However, due to a lack of appropriate data, no explicit account can be taken of the incomplete dissolution of carbides during austenitisation. Failure to do this should reflect in a greater uncertainty in the predictions that are made using the trained neural networks. A total of 1910 experimental data were collected from published literature [13–52] and digitised. Table 2 shows a selection of ductile iron alloys included in the database.

In discussing the microstructure, we shall distinguish between the volume fraction of residual austenite ($V_{r\gamma}$),

Table 1
The variables used to develop the neural network model

Input element	Minimum	Maximum	Mean	Standard deviation
Carbon (wt.%)	2.3	3.97	3.58	0.165
Silicon (wt.%)	1.57	3.78	2.57	0.21
Manganese (wt.%)	0.01	1.52	0.34	0.23
Molybdenum ^a (wt.%)	0.0	0.74	0.16	0.17
Nickel ^a (wt.%)	0.0	3.82	0.29	0.53
Copper ^a (wt.%)	0.0	1.60	0.23	0.29
Austenitising temperature (°C)	800	1050	900	34
Austenitising time (min)	15	240	97	34
Austempering temperature (°C)	230	455	350	39
Austempering time (min)	0.5	60000	1039	5625
Austempering time $\ln \{t_A/s\}$	1.477	6.556	3.659	0.948
$\ln \{-\ln \{V_\gamma\}\}$	-0.875	2.03	0.414	0.418

^a Molybdenum, nickel and copper were frequently not reported in publications since they were not deliberate additions, in which case their concentrations were set to zero.

Table 2
A selection of alloys intended to illustrate the range covered in the database used to create the neural network model

C	Si	Mn	Mo	Ni	Cu	V	Cr	Ti	Ref
3.63	2.54	0.36	0.01	0.07	0.04	0	0.04	0	[14]
3.67	2.45	0.20	0.30	0	0.78	0	0	0	[17]
3.3	2.5	0.21	0	1.6	1.6	0	0	0	[16]
3.16	2.82	0.96	0	0	0.07	0.02	0	0	[18]
3.56	2.33	0.57	0.06	0.1	0	0.04	0	0	[26]
3.66	2.51	0.53	0.26	1.34	0	0	0	0	[30]
3.7	2.52	0.44	0.01	0.06	0.06	0	0.05	0	[29]
3.53	2.44	0.5	0.25	0	1.37	0	0	0	[55]
3.51	2.81	0.25	0.13	0	0.39	0	0	0	[33]
2.5	2.0	0.74	0	3.8	0	0	0.02	0	[42]
3.3	2.2	0.37	0	0	0	0	0	0	[22]
3.52	2.64	0.67	0.25	0	0.25	0	0	0	[34]

which is the untransformed austenite at the austempering temperature, and the volume fraction of retained austenite ($V_{\gamma r}$) which remains untransformed at ambient temperature. One approach is to use the neural network with the austempering time as the input. However, this is not justified metallurgically since the fraction is not expected to vary linearly with time, but as the logarithm of time. The evolution of volume fraction with time in nucleation and growth reactions follows a sigmoidal behaviour. This is because the bainite reaction associated with the first stage of austempering, and indeed, the subsequent decomposition of the austenite in stage two, should both follow an Avrami type equation with

$$\zeta = 1 - \exp\{-k_A t^n\}, \quad (2)$$

where ζ is the fraction of transformation. The detailed values of the Avrami parameter k_A and the time exponent n will depend on many different factors, as reviewed by Christian [53]. If ζ is the fraction of bainitic ferrite then $V_\gamma = 1 - \zeta$ during stage I, so it is expected that

$$\ln \{-\ln \{V_\gamma\}\} \propto \ln \{t_A\}. \quad (3)$$

Interestingly, since it is the residual austenite which undergoes transformation to carbides and ferrite during stage II, the relationship implied in Eq. (3) also applies there.

It follows that it is natural to use $\ln\{-\ln\{V_\gamma\}\}$ as the output parameter in the neural network analysis, rather than $V_{\gamma r}$ directly. The former is physically justified on the basis of the Avrami equation, but is additionally important because $V_{\gamma r}$ and its associated error calculations become bounded between zero and one for all positive values of t , as they should be. This will become apparent later in the paper.

On a similar rationale, the time parameter in the input set should be $\ln\{t_A\}$ rather than t_A . However, it is conceivable that there might be some unknown process which varies directly with t_A so both the logarithmic time and the time were included as input variables. This has the advantage of avoiding bias in the inputs; the method used here has automatic relevance determination [8] and hence sets the weights associated with an

irrelevant input to small or zero values should that be justified.

It is emphasised that unlike linear regression analysis, the ranges stated in Table 1 cannot be used to define the range of applicability of the neural network model. This is because the inputs are in general expected to interact. We shall see later that it is the Bayesian framework of our neural network analysis which makes possible the calculation of error bars whose magnitudes vary with the position in the input space, which define the range of useful applicability of the trained network. A visual impression of the spread of the data is shown in Fig. 3.

4. Analysis

All the variables were normalised within a range of ± 0.5 as follows:

$$x_N = \frac{(x - x_{\min})}{(x_{\max} - x_{\min})} - 0.5, \quad (4)$$

where x_N is the normalised value of x , which has the minimum and maximum values given by x_{\min} and x_{\max} , respectively. The normalisation is not necessary for the analysis but facilitates the subsequent comparison of the significance of each of the variables.

The database was randomised and then partitioned equally into test and training data sets. The latter was used to create a large variety of neural networks models whereas the test data set was used to see how the trained models generalised on unseen data.

Training involves the derivation of the weights by the minimisation of the regularised sum of squared errors σ_v . The complexity of the model is controlled by the number of hidden nodes, and the values of the regularisation constants [8], one associated with each input, one for biases and one for all weights connected to the output. The inferred noise level σ_v is expected to decrease as the number of hidden units (Fig. 4a). The number of hidden units is set by examining the performance of the model on unseen test data. The test set

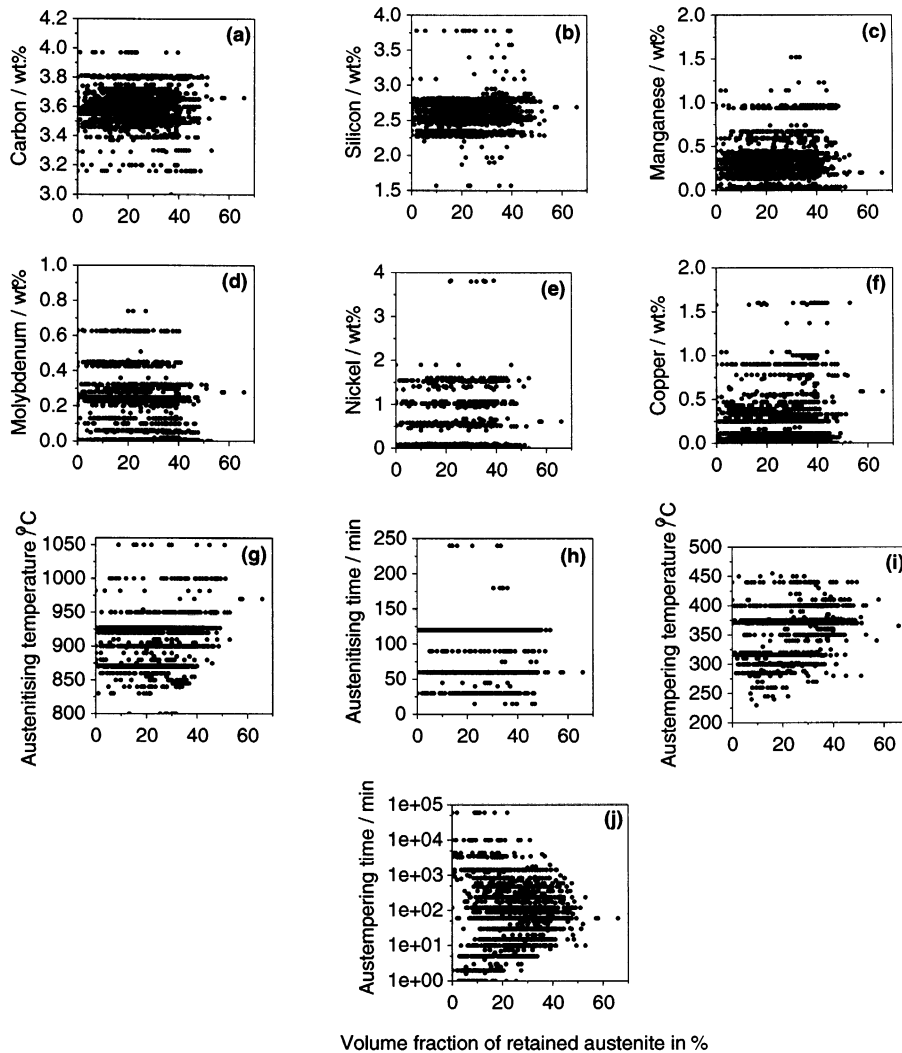


Fig. 3. The database values of each variable versus the volume fraction in % of retained austenite.

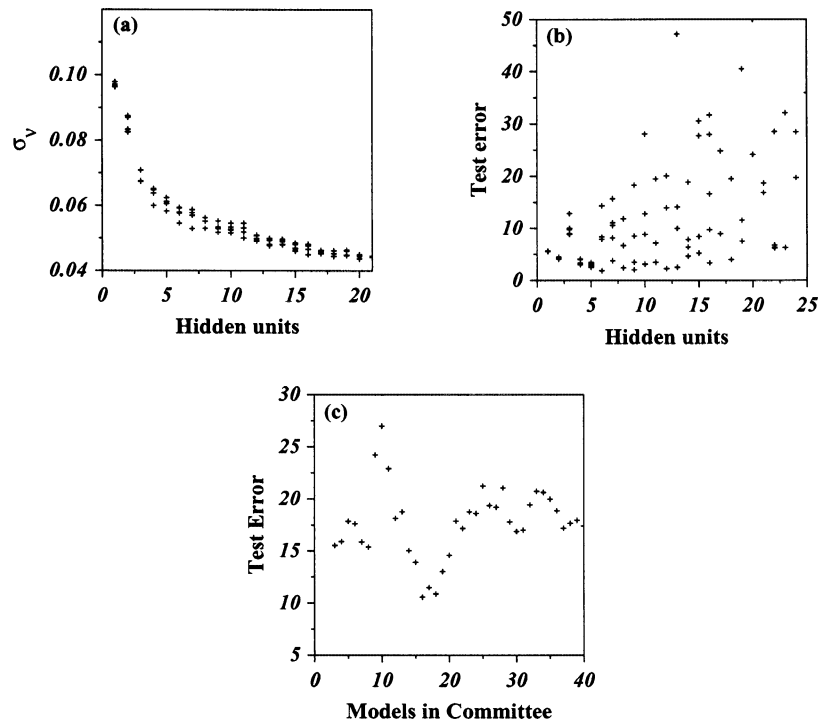


Fig. 4. (a) σ_v and (b) test error as a function of the number of hidden units; (c) the test error plotted as a function of the number of models in a committee of models.

error tends to go through a minimum at an optimum complexity (Fig. 4b).

It is possible that a committee of models can make a more reliable prediction than an individual model [54]. The best models are ranked using the values of the test errors. Committees are then formed by combining the predictions of the best L models, where $L = 1, 2, \dots$; the size of the committee is therefore given by the value of L . A plot of the test error of the committee versus its size L gives a minimum which defines the optimum size of the committee as shown in Fig. 4(c). The test error for a committee is calculated according to:

$$T_{\text{en}} = 0.5 \sum_n (\bar{Y}_n - t_n)^2, \quad \text{where} \quad \bar{Y}_n = \frac{1}{L} \sum_l y_n^{(l)}. \quad (5)$$

The test error associated with the best single model is greater than that of any of the committees. However, the committee with sixteen models was found to have an optimum membership with the smallest test error (Fig. 4c). Once the optimum committee is chosen, it is re-trained on the entire dataset without changing the complexity of each model, with the exception of the inevitable and relatively small adjustments to the weights. Fig. 5 shows normalised predicted values versus experimental values for the best model in the training and test datasets. The predictions made using the optimum committee of models are illustrated in Fig. 5(c).

Fig. 6 illustrates the significance of each of the input

variables, as perceived by the neural network, in influencing the retained austenite content. The magnitude of the significance is a measure of the extent to which a particular input explains the variation in the retained austenite content. As expected, the austempering time and temperature, and the austenitisation temperature feature prominently.

5. Application of the model

The neural network can capture interactions between the inputs because the functions involved are non-linear. The nature of these interactions is implicit in the values of the weights, but the weights are not always easy to interpret. For example, there may exist more than just pairwise interactions, in which case the problem becomes difficult to visualise from an examination of the weights. A better method is to actually use the network to make predictions and to see how these interactions depend on various combinations of inputs.

Unlike linear regression analysis, the range of applicability of a neural network model cannot be defined in terms of the range of the data used to create the model. This is because the network is non-linear so the inputs will in general be expected to interact. It is the Bayesian framework of the present method which resolves this problem because it allows the calculation of error bars

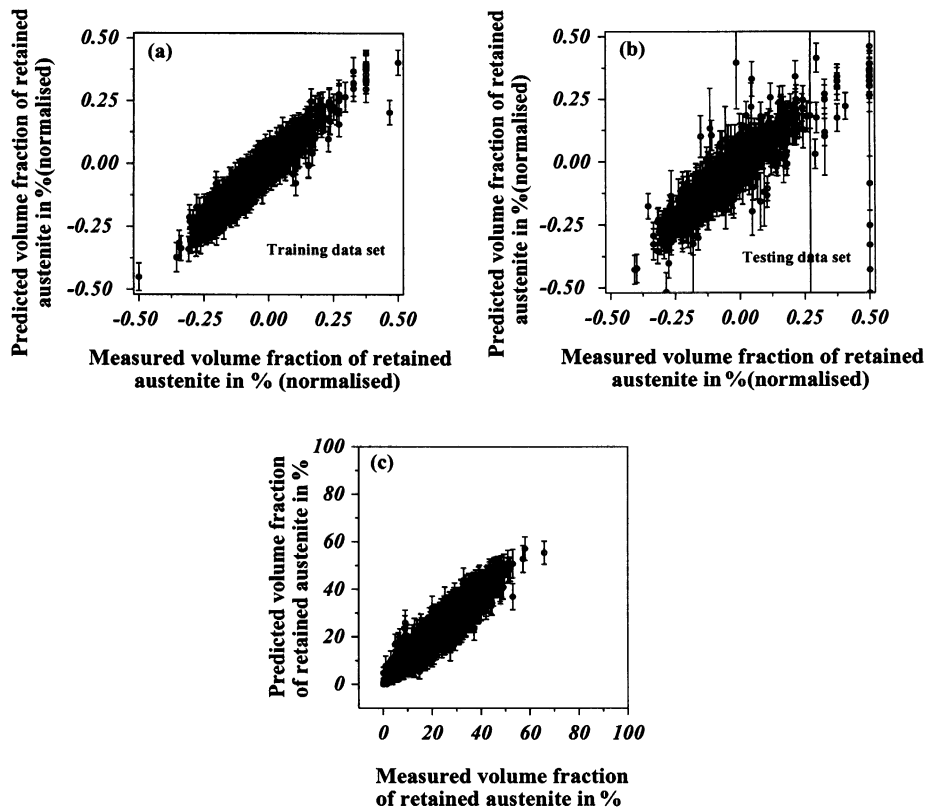
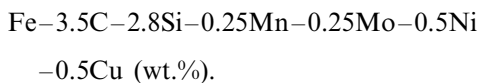


Fig. 5. Predictions made using the best model, selected as the one having the smallest test error. (a) Training data set. (b) Test data set. (c) Predictions made on the entire dataset using the optimum committee.

which define the range of useful applicability of the trained network. The model can therefore be used in extrapolation given that it indicates appropriately large uncertainties when knowledge is sparse.

The basic cast iron chosen to study the variations has the chemical composition



According to the literature [55–58] this should have a low tendency to form intercellular carbides; at the same time, chemical segregation should not be excessive. The austemperability is expected to be around 34.3 mm in diameter, calculated using a relationship due to Lee and Voigt [59]. Unless otherwise stated, the heat treatment parameters used are $T_\gamma = 900^\circ\text{C}$, $t_\gamma = 60$ min, $T_A = 370^\circ\text{C}$ and $t_A = 60$ min.

Fig. 7 illustrates the effect of two different austenitising temperatures on the calculated quantity of retained austenite. Consistent with the first stage reaction, $V_{\gamma r}$ at first increases, but then starts to decrease with the onset of stage II which is connected with carbide precipitation. Calculations like these can easily be used to define the heat treatment window, which is marked on each of the plots.

Although the influence of T_γ will be discussed in more detail later, Fig. 7(a) shows that for an austenitising temperature of 900°C , the end of stage I reaction occurs after approximately 30 min whilst for $T_\gamma = 950^\circ\text{C}$ (Fig. 7b) it happens after some 50 min. This behaviour has been explained by several researchers [60,61]. A decrease in T_γ accelerates the bainite reaction kinetics because it leads to a reduction in the equilibrium carbon concentration of the austenite. Consequently, the amount of austenite that is retained is reduced, as predicted by the model.

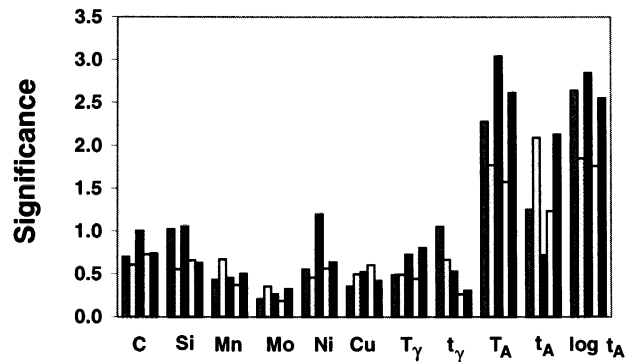


Fig. 6. Model perceived significance of input parameters in the best five models from the committee trained on the volume fraction of retained austenite. σ_w values are presented for each variable.

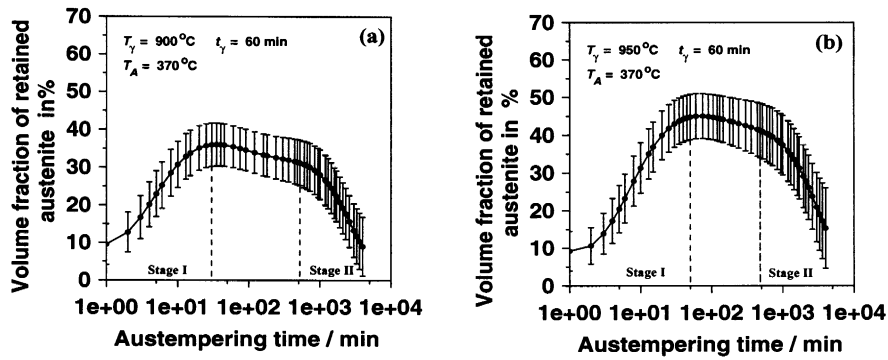


Fig. 7. Predictions of volume fraction of retained austenite in % as a functions of austempering time for an alloy Fe-3.5C-2.8Si-0.25Mn-0.25Mo-0.5Ni-0.5Cu (wt.%), at: (a) $T_\gamma = 900^\circ\text{C}$; and (b) at $T_\gamma = 950^\circ\text{C}$.

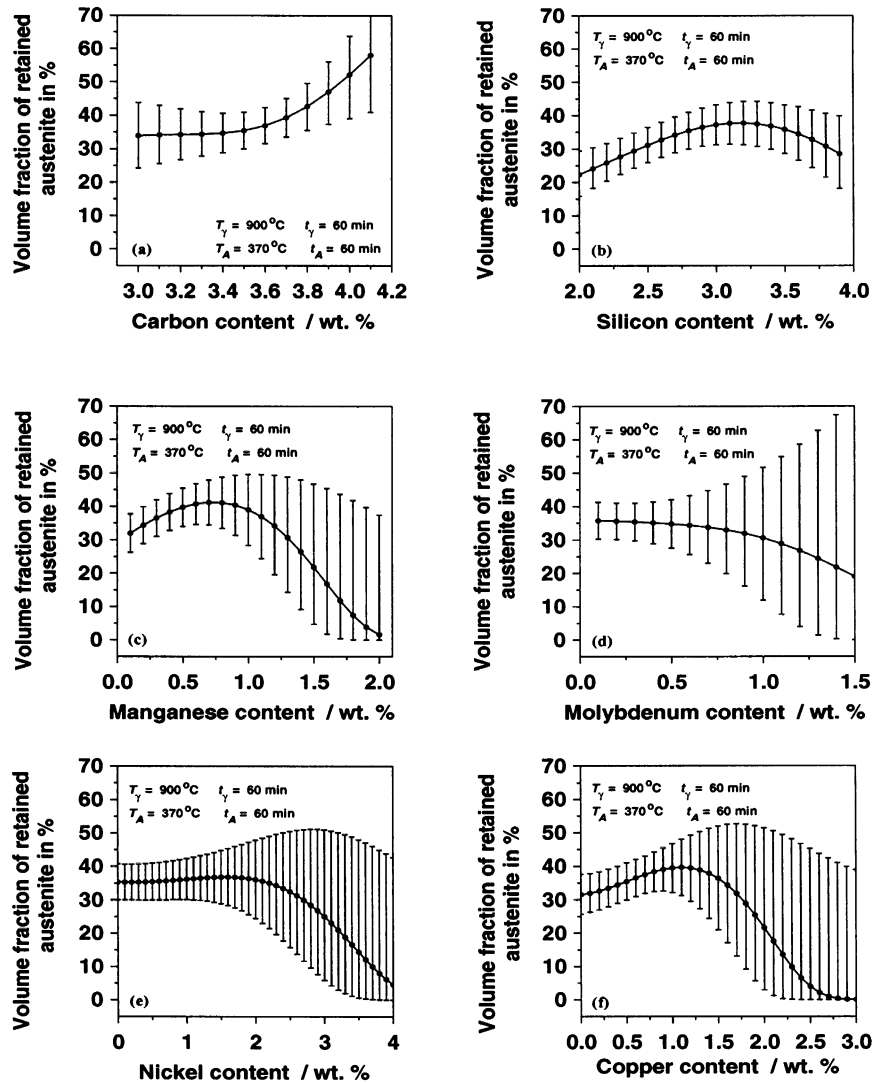


Fig. 8. Predictions of volume fraction of retained austenite in % as a function of chemical composition (Basic cast iron: Fe-3.5C-2.8Si-0.25Mn-0.25Mo-0.5Ni-0.5Cu wt.%).

5.1. Carbon

Fig. 8(a) shows that $V_{\gamma r}$ hardly changes as the carbon

concentration of the cast iron (\bar{x}) is increased from 3.1 to 3.7 wt.%. In an ideal Fe-C binary cast iron, there should be no change in the equilibrium carbon concen-

tration of the austenite (x_γ) as the average concentration \bar{x} is increased, although there would be an increase in the fraction of graphite. However, the cast iron studied is not a binary alloy but contains many other elements which give the material additional degrees of freedom according to the phase rule. In such a multicomponent system, a change in \bar{x} may in fact alter x_γ .

Such effects can be studied using MTDATA which is a computer program that in combination with the SGTE database [62] permits the calculation of phase diagrams in multicomponent, multiphase systems. Table 3 shows the results of those MTDATA calculations in our cast iron allowing for just two phases (FCC and free graphite) at the austenitising temperature. The results do reveal that the equilibrium value of x_γ at 900°C remains almost constant, but there is a slight decrease as \bar{x} is increased.

The same figure (Fig. 8a) shows that there is a significant rise in retained austenite beyond 3.6 wt.%. Although there is little information to support this behaviour, a possible answer would be that it takes longer for equilibrium to be reached when \bar{x} is large.

5.2. Silicon

Silicon levels in excess of 2 wt.% are generally recommended for ductile irons; the silicon promotes graphite formation but equally importantly, it is essential to delay the precipitation of cementite. This leads to the development of the mixed bainitic ferrite and carbon-enriched austenite microstructure which is so beneficial to the mechanical properties of ADI [63]. An increase in the Si concentration from 2.5 to 3.1 wt.% has been shown to delay the onset of the stage II reaction from 70 min to 4.5 h [58]. This might allow for more bainitic transformation and consequently more austenite carbon enrichment without precipitation of carbide. Therefore, an increase in retained austenite is expected as is observed in Fig. 8(b). However, beyond 3.2 wt.% Si, which seems to be the optimum silicon content, there is a drop in retained austenite. This might be caused by the formation of islands of pro-eutectoid ferrite in the bainite structure as found by Gagne [64] in his experiments for an ADI with 3.7 wt.% Si austenitised at the same temperature as in Fig. 8(b) (900°C). The eutectoid temperature for this alloy is around 858°C [64], assuming a homogeneous alloy. However, in practice there will be some regions where the silicon concentration

could be higher than 3.7 wt.% and eutectoid temperature near 900°C [64,65].

5.3. Manganese

Manganese is added to ductile iron primarily to improve its hardenability, but it has a pronounced tendency to segregate during solidification, thereby causing the precipitation of complex Fe–Mn carbides at solidification-cell boundaries [30,58,66].

Fig. 8(c) shows that beyond about 0.7 wt.%, manganese leads to a reduction in the quantity of retained austenite. This is easily understood because it greatly retards both the kinetics of the bainite reaction and the maximum amount of bainite that can form at any temperature [67], thereby reducing the extent to which austenite can be enriched with carbon. This, of course, reduces the stability of the residual austenite to martensitic transformation, causing the decline in $V_{\gamma r}$.

5.4. Molybdenum, copper and nickel

Molybdenum has a powerful influence on the hardenability of ductile irons and so is an essential alloying element for the production of large components. However, like manganese, it segregates at cell boundaries during solidification to form carbides. The use of molybdenum should thus be limited. The molybdenum carbides are very stable and hardly dissolve during austenitisation.

Consistent with experimental data [68], Fig. 8(d) shows that for concentrations less than 0.5 wt.%, molybdenum has hardly any effect on the retained austenite content; the predictions are too uncertain for larger concentrations.

It has been argued [29,57] that the net effect of molybdenum is to delay stage II although there are contradictory reports from BCIRA [69]. The present model can be used to clarify this. Fig. 9 shows with considerable certainty that there is no major difference between irons containing different molybdenum concentrations except for very long austempering times, where the alloy richest in molybdenum is more resistant to stage II decomposition.

There are contradictory claims about the influence of copper on the retained austenite content [63,68]. The present model, which is based on the analysis of a very large database, shows that copper does indeed stabilise austenite and hence leads to a greater fraction of re-

Table 3

Carbon content of austenite (x_γ) at 900°C calculated using MTDATA with SGTE database, for an iron of composition Fe–C–2.8Si–0.25Mn–0.25Mo–0.5Ni–0.5Cu (wt.%)

C (wt.%)	3.1	3.2	3.3	3.4	3.5	3.6	3.7	3.8	3.9	4.0
x_γ (wt.%)	0.7830	0.7826	0.7822	0.7818	0.7813	0.7809	0.7805	0.7801	0.7797	0.7793

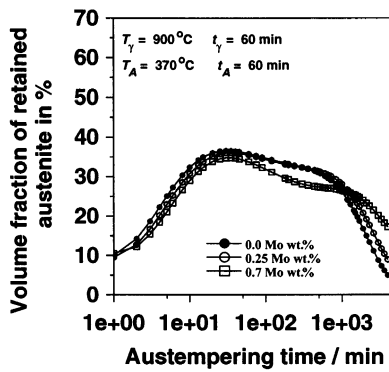


Fig. 9. Influence of molybdenum on the retained austenite content for an iron Fe-3.5C-2.8Si-0.25Mn- x Mo-0.5Ni-0.5Cu (wt.%).

tained austenite at concentrations less than 1 wt.%. Naturally, any element which increases the hardenability (e.g. Mn, Ni, Cu) will retard the bainite reaction so that excessive alloying must eventually lead to a smaller V_{ret} , as is apparent in Fig. 8(f).

Nickel is usually added to improve hardenability since copper alone does not provide sufficient hardenability to successfully austemper thick castings. However, as shown in Fig. 8(e) nickel concentrations less than 2 wt.% does not seem to have any influence on retained austenite as copper does seem to have. More experiments are needed for nickel concentrations higher than 2 wt.%. This is inferred from the large error bars.

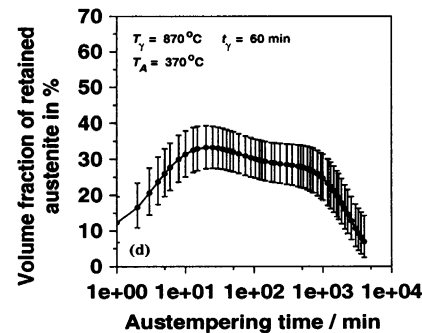
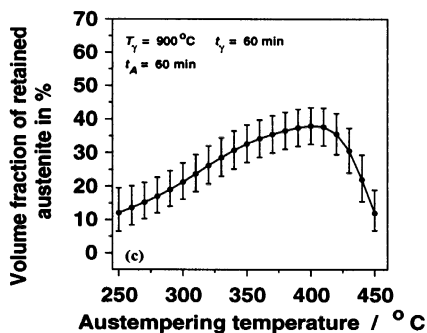
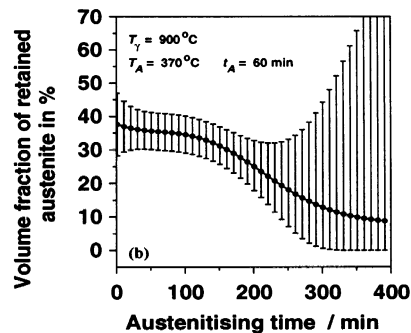
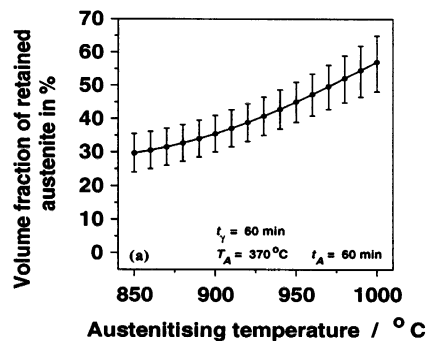


Fig. 10. Predictions of volume fraction of retained austenite in % as a function of the heat treatment conditions (Basic cast iron: Fe-3.5C-2.8Si-0.25Mn-0.25Mo-0.5Ni-0.5Cu wt.%).

5.5. Austenitising conditions

The austenitising temperature and time determines the carbon concentration x_{γ} of austenite which is in equilibrium with the graphite at T_{γ} . Austenitisation must therefore greatly influence the stability of the austenite, as is evident from Fig. 10(a). A higher T_{γ} corresponds to a larger x_{γ} . The effect of austenitisation time is less significant for $t_{\gamma} < 200$ min and the large error bars associated with longer times indicate a need for experiments. The effect of t_{γ} is small, presumably because equilibrium is established fairly quickly at these temperatures.

5.6. Austempering conditions

There are clearly major effects of T_A and t_A on the fraction of austenite that is retained at ambient temperature (Fig. 10). The predicted effects are precisely those expected.

Considering first the effect of austempering temperature, the fraction of bainite that can form is smallest at temperatures close to the bainite-start temperature B_S [66]. Consequently, the retained austenite content is close to zero at high temperatures. It increases as more bainite is able to form with increasing undercooling below B_S . The maximum arises because of two competitive effects: whereas an increase in the fraction of bainite raises x_{γ} , the bainite also consumes austenite so that less remains to be retained. Thus, at the lower

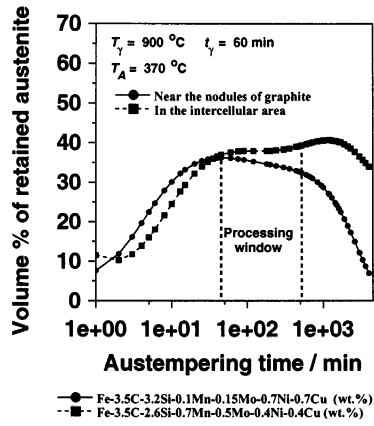


Fig. 11. Predictions of volume fraction of retained austenite in % for our study's alloy taking into account segregation of alloying elements towards nodules of graphite and intercellular area.

temperatures, the latter effect dominates leading to a fall in the amount of retained austenite.

The effect of the austempering time is straightforward, that there are the stage I and II phenomena which lead to the behaviour illustrated in Fig. 10(d).

5.7. Segregation effects

The effect of chemical segregation is illustrated in Fig. 11, by conducting calculations for typical matrix compositions in the vicinity of a graphite nodule and along the midpoint between adjacent nodules.

Notice that the curve which describes the intercellular region has less stable austenite than that for the vicinity of the nodules of graphite (Fig. 11). This is expected since the silicon concentration is the lowest in the intercellular region and manganese is the highest.

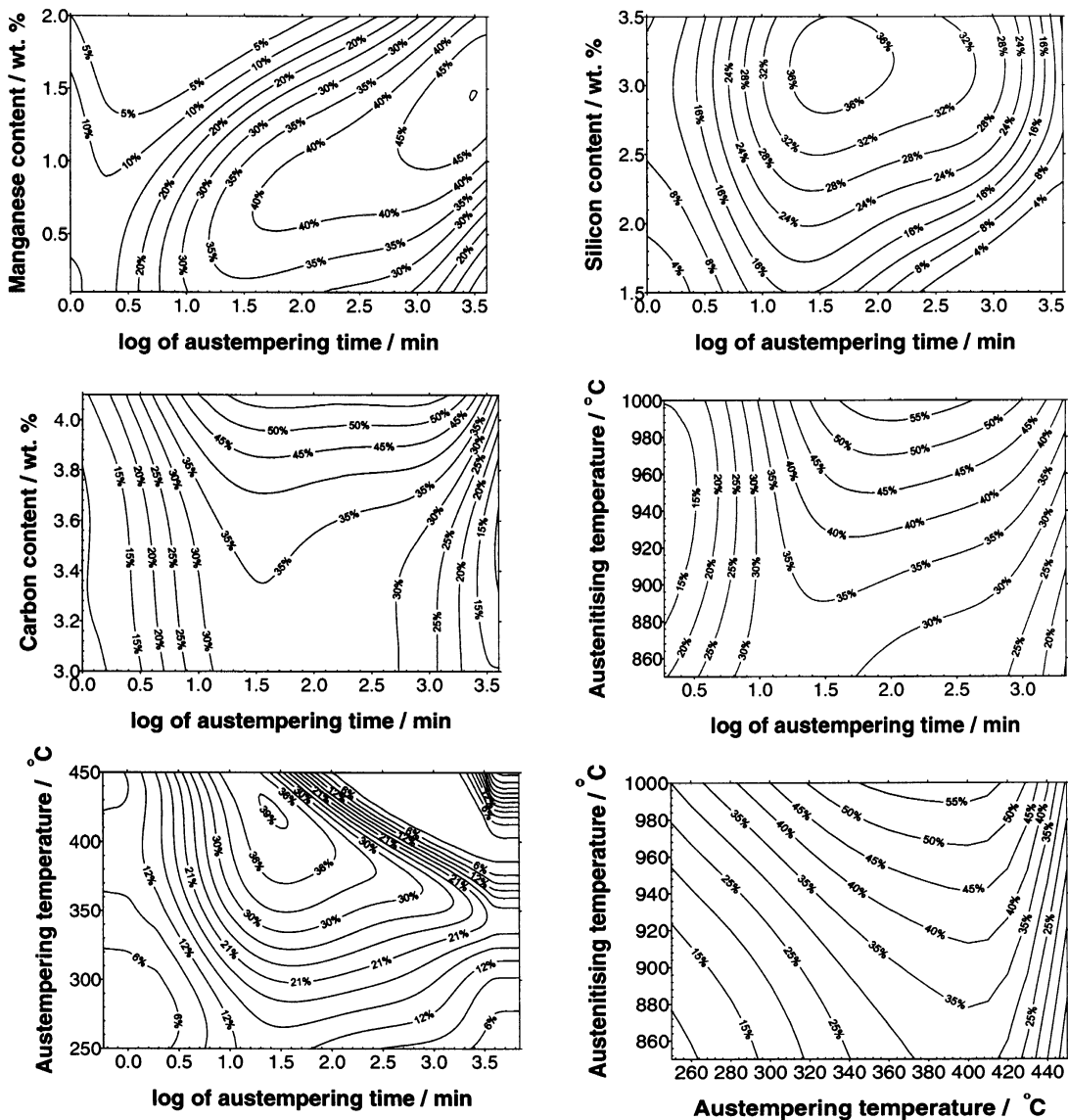


Fig. 12. Contour plots of the volume fraction of retained austenite in % for (Fe–3.5C–2.8Si–0.25Mn–0.25Mo–0.5Cu) using $T_\gamma = 900^\circ\text{C}$, $t_\gamma = 60$ min, $T_A = 350^\circ\text{C}$, $t_A = 60$ min. The error bars associated with these predictions have been omitted for the sake of clarity.

5.8. Contour plots

Fig. 12 shows some contour plots, many of which enable the selection of conditions for the optimisation of the fraction of retained austenite by visual inspection. The effect of manganese is remarkable since as manganese increases the field of maximum retained austenite is reduced dramatically as well as shifted towards longer times, consistent with the previous discussion about its effect on hardenability.

6. Summary

A neural network model has been developed to enable the estimation of the fraction of retained austenite in austempered ductile cast irons as a function of their chemical composition (C, Mn, Si, Ni, Mo, Cu), and the austenitisation and austempering parameters. The model successfully reproduces many experimentally observed trends. It can be exploited in two ways, first in the design of cast irons and their heat treatments, but also to identify whether experiments are needed in the future. If the model prediction is associated with a large uncertainty than an experiments can be considered to be novel and useful.

The computer program associated with this work can be obtained freely from the Materials Algorithms Project Library on: <http://www.msm.cam.ac.uk/map/mapmain.html>

Acknowledgements

The authors are grateful to Professor Alan Windle for the provision of laboratory facilities at the University of Cambridge. One of the authors (M. A. Yescas) would like to thank the National Council of Science and Technology from Mexico (CONACYT) for a scholarship.

References

- [1] K.B. Rundman, R.C. Klug, AFS Trans. 90 (1982) 499–508.
- [2] R.C. Voigt, AFS Trans. 92 (1983) 253–262.
- [3] E. Dorazil, B. Barta, E. Munsterova, Giessereitechnik 19 (1973) 79–83.
- [4] W.S. Owen, Trans. ASM 46 (1954) 812–829.
- [5] R.F. Hehemann, K.R. Kinsman, H.I. Aaronson, Metall. Trans. 3 (1972) 1077–1094.
- [6] R.C. Voigt, Cast. Met. 2 (2) (1989) 72–93.
- [7] D.J. Moore, T.N. Rouns, K.B. Rundman, AFS Trans. 94 (1986) 255–264.
- [8] D.J.C. MacKay, In: H. Cerjack, (Ed.), 'Mathematical Modelling of Weld Phenomena 3', Graz, Austria, 1997, p. 359.
- [9] H. Fuji, H.K.D.H. Bhadeshia, ISIJ Int. 39 (10) (1999) 965–979.
- [10] R.C. Eberhart, R.W. Dobbins, Neural Networks PC tools, Academic Press, California, 1990.
- [11] D.J.C. MacKay, Neural Computation 4 (1992) 415.
- [12] D.J.C. MacKay, Neural Computation 4 (1992) 448.
- [13] S.E. Stenfors, J. Storesun, R. Sandstrom, 2nd International Conference on Austempered Ductile Iron, University of Michigan, (1986), pp. 227–236.
- [14] K.B. Rundman, D.J. Moore, K.L. Hayrynen, W.J. Dubensky, T.N. Rouns, J. Heat Treating 5 (2) (1988) 79–95.
- [15] N. Varahraam, O. Yanagisawa, Cast. Met. 3 (3) (1990) 129–139.
- [16] M. Grech, J.M. Young, Cast. Met. 3 (1990) 98–103.
- [17] W.S. Zhou, Q.D. Zhou, S.K. Meng, Cast. Met. 6 (2) (1993) 69–75.
- [18] M.N. Ahmadabadi, Cast. Met. 5 (2) (1992) 62–72.
- [19] J.M. Prado, A. Pujol, J. Cullerell, J. Tartera, Mater. Sci. Technol. 11 (1995) 294–298.
- [20] G.J. Cox, Br. Foundryman, 79 (1986) 215–219.
- [21] T. Takahashi, T. Abe, S. Tada, Metall. Mater. Trans. A 27A (1996) 1589–1598.
- [22] N. Darawish, R. Elliott, Mater. Sci. Technol. 9 (1993) 572–585.
- [23] W.J. Dubensky, K.B. Rundman, AFS Trans. 93 (1985) 389–394.
- [24] J. Aranzabal, I. Gutierrez, J.J. Urcola, Mater. Sci. Technol. 10 (1994) 728–737.
- [25] M.M. Shea, E.F. Ryntz, AFS Trans. 94 (1986) 683–688.
- [26] D.J. Moore, T.N. Rouns, K.B. Rundman, AFS Trans. 94 (1986) 255–264.
- [27] D.J. Moore, T.N. Rouns, K.B. Rundman, AFS Trans. 93 (1985) 705–718.
- [28] T.N. Rouns, K.B. Rundman, D.M. Moore, AFS Trans. 92 (1984) 815–840.
- [29] T.N. Rouns, K.B. Rundman, AFS Trans. 95 (1987) 851–874.
- [30] E. Dorazil, T. Podrabsky, J. Svejcar, AFS Trans. 98 (1990) 765–774.
- [31] M. Grech, J.M. Young, AFS Trans. 98 (1990) 345–353.
- [32] G. Nadkarni, A.H. Behraves, R.D. Warda, K.G. Davis, M. Sahoo, AFS Trans. 103 (1995) 93–101.
- [33] S. Yazadani, R. Elliott, Mater. Sci. Technol. 15 (1999) 531–540.
- [34] H. Bayati, R. Elliott, G.W. Lorimer, Mater. Sci. Technol. 11 (1995) 776–786.
- [35] R. Boschen, H. Vettters, P. Mayr and P.L. Ryder, Practical Metall. 15 (1988) 524–531.
- [36] C.T. Chen, T.S. Lei, Int. J. Cast. Met. Res. 10 (1997) 117–123.
- [37] H. Bayati, R. Elliott, Mater. Sci. Technol. 11 (1995) 118–129.
- [38] N. Darawish, R. Elliott, Mater. Sci. Technol. 9 (1993) 586–602.
- [39] M. Gagne, P.A. Fallon, Can. Metall. Q. 25 (1) (1986) 79–90.
- [40] A.S. Hamid, R. Elliott, Mater. Sci. Technol. 12 (1996) 1021–1031.
- [41] R. Kazerooni, A. Nazarboland, R. Elliott, Mater. Sci. Technol. 13 (1997) 1007–1015.
- [42] T. Kobayashi, H. Yamamoto, Metall. Trans. A 19A (1988) 319–327.
- [43] C.K. Lin, J.Y. Wei, Mater. Trans. JIM 38 (8) (1997) 682–691.
- [44] A. Owhadi, J. Hedjazi, P. Davami, Mater. Sci. Technol. 14 (1998) 245–250.
- [45] S.K. Putatunda, P.K. Gadicherla, Mater. Sci. Eng. A286 (1999) 15–31.
- [46] P. Prasad, S.K. Putatunda, Metall. Mat. Trans. A 28A (1997) 1457–1470.
- [47] P. Prasad, S.K. Putatunda, Metall. Mat. Trans. A 29A (1998) 3005–3016.
- [48] I. Schmid, A. Schuchert, Z. Metallkde 78 (1987) 871–875.
- [49] S.M. Shah, J.D. Verhoeven, Wear 113 (1986) 267–278.
- [50] P. Shanmugam, P. Prasad, K.U. Rajendra, N. Venkataraman, J. Mater. Sci. 29 (1994) 4933–4940.

- [51] A. Trudel, M. Gagne, *Metall. Q.* 36 (5) (1998) 289–298.
- [52] T.S. Shih, Z.C. Yang, *Int. J. Cast. Met. Res.* 10 (1998) 335–344.
- [53] J.W. Christian, *Theory of Transformations in Metals and Alloys Part 1*, 2nd, Pergamon Press, Oxford, 1975.
- [54] D.J.C. MacKay, *Neural Computation* 4 (4) (1992) 698.
- [55] E. Dorazil, 'Ellis Horwood Series in Metals and Associated Materials', In: E.G. West (Ed.), Obe (1991), pp. 43–47.
- [56] T.N. Rouns, K.B. Rundman, *AFS Trans.* 95 (1987) 851–874.
- [57] Y. Ueda, M. Takita, 2nd International Conference on Austempered Ductile Iron, University of Michigan, (1986), pp. 141–147.
- [58] R.C. Voigt, *Cast. Met.* 2 (2) (1989) 72–93.
- [59] Y.H. Lee, R.C. Voigt, *AFS Trans.* 97 (1989) 915–938.
- [60] N. Darawish, R. Elliott, *Mater. Sci. Technol.* 9 (1993) 586–602.
- [61] H. Bayati, R. Elliott, G.W. Lorimer, *Mater. Sci. Technol.* 11 (1995) 776–786.
- [62] MTDATA, Metallurgical and thermomechanical databank, National Physical Laboratory, Teddington, Middx, UK (1995)
- [63] R. Elliott, *Cast Iron Technology*, Butterworths, 1988, pp. 140–152.
- [64] M. Gagne, *AFS Trans.* 93 (1985) 801–812.
- [65] E. Schurmann, J. Von Hirsch, *Giesserei* 53 (1966) 398–400.
- [66] B.V. Kovacs, 2nd International Conference on Austempered Ductile Iron, University of Michigan, (1986) pp. 291–296.
- [67] H.K.D.H. Bhadeshia, *Bainite in Steels*, The Institute of Materials, 1992.
- [68] Y. Mi, *Scripta Metall. Mater.* 32 (9) (1995) 1313–1317.
- [69] R. Harding, 2nd International Conference on Austempered Ductile Iron, University of Michigan, (1986), pp. 39–54.